ACS OMEGA

Open Access

http://pubs.acs.org/journal/acsodf

Article

Nonlinear Optical Response of Tetrel-Modified Tetraphenyl-Adamantane Clusters

Ferdinand Ziese* and Simone Sanna*

Cite This: *ACS Omega* 2024, 9, 49816−49824

Read Online

ACCESS | Metrics & More | Article Recommendations | Supporting Information

ABSTRACT: The second harmonic generation (SHG) properties of adamantane-based tetraphenyl clusters are predicted from first principles and analyzed on the basis of the involved electronic transitions. In particular, the effect of a tetrel substitution in the cluster core on the nonlinear optical response is investigated. Electronic transitions spatially localized at the substituents are found to be responsible for the optical nonlinearities. The intensity of the SHG signal grows with the atomic number of the considered tetrel. As the substitution does not distort the cluster core or substantially alter its symmetry, the enhanced SHG intensity is traced to a higher electron density at the substituents. The latter results in a larger spatial overlap of the states involved in the electronic transitions, which increases their probability. The presented results provide a theoretical foundation for the design of tailored nonlinear optical sources.

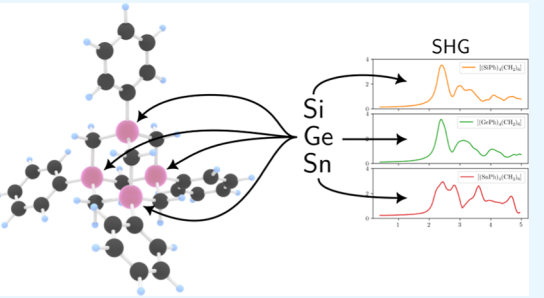

INTRODUCTION

Adamantane-based clusters with organic substituents are generally characterized by a strong nonlinear optical response.[1] Several clusters in this material class are able to convert infrared radiation into directed white light,[2−4] while other adamantane-based clusters feature a pronounced second harmonic generation (SHG).[5] Due to their appealing properties and possible applications in a variety of technologies,[6,7] the adamantane-based clusters with organic substituents (as well as related compounds) have been studied experimentally[8−13] and theoretically.[14,15] Recent publications report, in particular, on attempts to synthesize the compounds in the form of glasses[16] and understand the origin of the optical response.[17,18] In ref 18, a general analysis procedure was proposed, which allows us to determine which orbital groups are involved in the electronic transitions leading to the calculated nonlinear optical signatures. Despite such a large effort, a comprehensive understanding of the materials class has not yet been achieved, and huge differences in the linear and nonlinear optical response of structurally and chemically very similar clusters remain puzzling.

In this work, we focus on a particular subset of adamantane-based molecules (Figure 1). Namely, we calculate the nonlinear optical response of tetrel-modified tetraphenyl adamantane clusters with the formula unit $[(RPh)_4(CH_2)_6]$ with R = C, Si, Ge, and Sn and adopt the analysis procedure of ref 18 to explore how the substitution influences the SHG spectra. Due to their toxicity, lead-containing compounds are less appealing as functional materials, and the cluster with R = Pb is not investigated in this work.

Our calculations reveal that the optical nonlinearities in the technologically relevant energy window between 0 and 3 eV

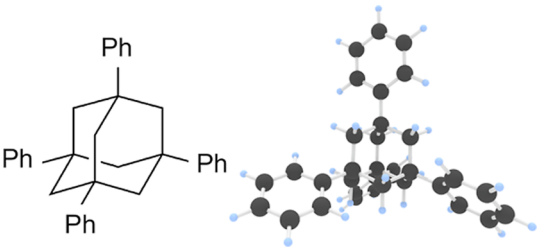

Figure 1. $[AdPh_4]$ adamantane-core molecule with phenyl substituents (C atoms in black and H atoms light blue). Considering different tetrel atoms connected to the phenyl rings leads to the general formula unit $[(RPh)_4(CH_2)_6]$ of the clusters investigated in this work (with R = C, Si, Ge, and Sn).

have their origin in electronic transitions localized at the tetraphenyl substituents. Therefore, the SHG spectra of $[AdPh_4]$, $[(SiPh)_4(CH_2)_6]$, $[(GePh)_4(CH_2)_6]$, and $[(SnPh)_4(CH_2)_6]$ show the corresponding spectral features, although they may differ in position and intensity. The latter correlates with the atomic number of the substituting tetrel. As the isovalent tetrel substitution does neither deform the cluster core nor lower the overall symmetry, the enhancement of the SHG intensity cannot have its origin in the cluster geometry. Instead, we trace it to an increased electronic density at the

Received: September 17, 2024
Revised: November 5, 2024
Accepted: November 20, 2024
Published: December 5, 2024

substituents, where the electronic transitions occur that are responsible for the optical nonlinearities. The enhanced overlap between involved states increases the transition probability and thus the SHG intensity. The results provided in the present work demonstrate the possibility to tune the nonlinear optical response of adamantane-based tetraphenyl clusters and provide a theoretical foundation for the design of optimized optical sources.

METHODS

The calculation of the nonlinear optical response is one major challenge in theoretical materials science.[19−21] In the present work, the nonlinear optical properties of the investigated molecular structures are modeled from first principles through density functional-based calculations performed with the YAMBO code.[22] The optical response is estimated in the time domain[23] within the independent particle approximation (IPA). Previous theoretical investigations of small tetraphenyl molecules have suggested an almost complete compensation of electronic self-energy and exciton binding energy for the lowest optical excitation.[15] Thus, calculations at the density functional theory (DFT) level of accuracy may already provide a good estimate of the optical response. Yet, the results at the IPA level of accuracy must be still considered to be of qualitative nature. Numerical parameters, such as time step, total propagation time, or spectral broadening, are chosen to ensure convergence of the nonlinear optical spectra. All employed numerical values are given in the Supporting Information. The electronic ground state, representing the starting point for the subsequent nonlinear optics computations, was computed via DFT, as implemented by Quantum Espresso.[24,25] Thereby, SG15 ONCV potentials,[26,27] as well as the PBE functional,[28] were utilized. To simulate the molecules in the gas phase, the molecule-in-a-box approach is used, whereby the asymmetric box is designed to decouple periodic images of the clusters. Structural optimization is conducted using a force threshold for the Hellmann−Feynman forces to be ≤0.005 eV. We account for dispersion forces using the vdW DFT-D3 method with Becke−Johnson damping function[29,30] in all calculations.

RESULTS AND DISCUSSION

Figure 2 shows the calculated SHG spectra of the investigated clusters. They present roughly the same spectral signatures, although they might differ in intensity and (to a lesser extent) position.

All clusters feature a main major peak at about 2.2 eV−2.4 eV, half the HOMO−LUMO gap's energy. The latter ranges from 4.59 eV for R = C to 4.38 eV for R = Sn. The major peak is followed by a second peak in the range between 2.8 eV and 3.1 eV that appears more as a shoulder in the case of R = C. The presence of similar spectral features for the different compounds suggests that the optical nonlinearities have their origin in the substituent (common to all clusters), as we shall demonstrate at a later stage.

The intensity of the optical nonlinearities grows with the atomic number of the considered tetrel. In the case of R = Sn, part of the intensity of the first peak is redistributed to the second peak due to the spread of available electronic transitions across a wider energy range, as we will separately discuss at the end of this chapter.

As previous studies[31] have revealed that the SHG intensity of molecular clusters decreases with the core symmetry, we first focus on the geometry of the investigated compounds. In Table 1, the R−C bond lengths are listed. The bond length grows as expected with the atomic number of the considered tetrel, closely mirroring the sum of the covalent radii. The angles between the bonds are substantially preserved by tetrel substitution. Moreover, a symmetry analysis of the whole cluster reveals that all of the investigated compounds are rather close to the exact point group symmetry. The latter is given within a tolerance of the atomic coordinates ranging from 0.009 Å for the most symmetric compound to 0.024 Å for the less symmetric compound. This means that the cluster core is not distorted and the tetragonal symmetry is not affected by the substitution. The only effect of the substitution is a substantial expansion of the core volume, as shown in Table 2.

In order to estimate the cluster core volume, a convex hull's volume of the adamantane-like core is considered, whereby hydrogen atoms are discarded. The resulting volumes are in good agreement with ref 14. The symmetry conservation suggests that the origin of the enhanced nonlinear optical activity of clusters with heavier tetrels must reside in the electronic structure.

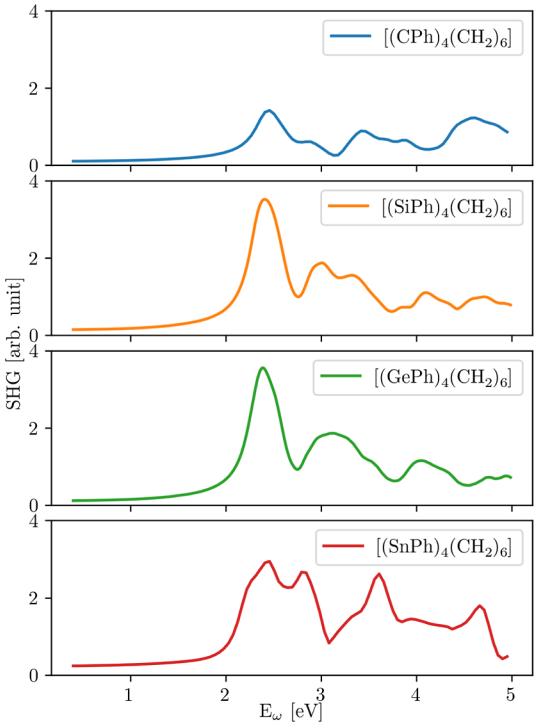

Figure 2. SHG response of modified adamantane-like core molecules with phenyl ligands with formula $[(RPh)_4(CH_2)_6]$ and R = C (blue), Si (orange), Ge (green), and Sn (red). The quantity shown on the *y*-axis is the averaged second-order hyperpolarizability coefficient $\chi^{(2)}_{jkl}(2\omega; \omega, \omega)$.

Table 1. Calculated Length of the R−C Bond in the Cluster Core

structure	bond length [Å]	%
$[(CPh)_4(CH_2)_6]$	1.54	100.00
$[(SiPh)_4(CH_2)_6]$	1.88	122.22
$[(GePh)_4(CH_2)_6]$	1.98	128.56
$[(SnPh)_4(CH_2)_6]$	2.17	140.96

https://doi.org/10.1021/acsomega.4c08541
ACS Omega 2024, 9, 49816−49824

Table 2. Calculated Volume of the Cluster Core of the Investigated Compounds

structure	core volume [Å^3]	%
$[(CPh)_4(CH_2)_6]$	9.3	100
$[(SiPh)_4(CH_2)_6]$	17.0	182.5
$[(GePh)_4(CH_2)_6]$	19.8	212.66
$[(SnPh)_4(CH_2)_6]$	26.1	279.81

$[(SiPh)_4(CH_2)_6]$. For an in-depth analysis of the electronic transitions related to the nonlinear optical response, we apply the procedure proposed in ref 18, which we briefly summarize in the following. The procedure is illustrated by the example of the $[(SiPh)_4(CH_2)_6]$ cluster, whose electronic structure and second-order optical response are shown in Figure 3.

In the left panel of Figure 3, the electronic energy levels of the orbital groups around the HOMO−LUMO gap are shown. We are interested in the electronic transitions from occupied orbital groups (named *origin* and labeled by o) to unoccupied orbitals (named *target* and labeled by t). We approximate the individual orbitals by grouping them into effective orbital groups for plots and interpretation if they are within an energy interval of ΔE = 0.1 eV.[1] The occupied orbital groups are colored alternately in lighter and darker gray colors to distinguish individual orbital groups more easily. The unoccupied orbital groups are color-coded individually instead. The origin orbitals are counted energy downward from the highest occupied one, while the target orbitals are counted upward. In the right panel, we consider electronic transitions from origin to target states by plotting the convolution $o * t$. The convolution is calculated for all origin orbital groups with a single target orbital group individually to simulate the electronic transitions. The convolution $o * t$ is color-coded as the considered target orbital and represented in histogram form in the right panel. The transparency is a rough indicator for a density of energy values.[2] The origin orbital groups in the left panel as well as the convolution in the right panel are shifted downward on the energy axis by the amount corresponding to the distance of the considered target orbital group to the LUMO. The SHG response is also shown in the right panel as a blue solid line, rotated, shifted, and scaled by a factor of 2 to share the energy axis of the electronic energy values. From top to bottom, $o * t$ is plotted for t = 0, t = 1, and t = 2.

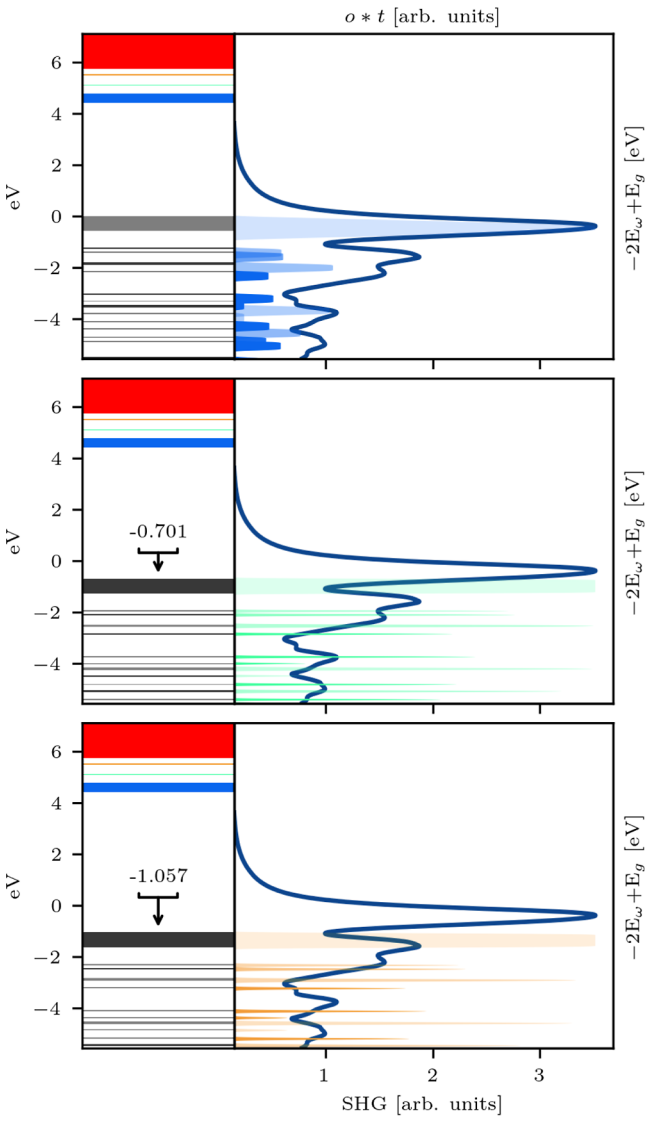

Figure 3. Orbital group energy values of $[(SiPh)_4(CH_2)_6]$ with corresponding scaled and shifted SHG response. The energy values of the origin (occupied) orbital groups are shifted for a direct transition to the respective target (unoccupied) orbital groups 0, 1, and 2.

Peaks of the convolution $o * t$ in correspondence of peaks of the SHG spectrum allow us to identify electronic transitions contributing to the SHG signatures. The electronic orbitals involved in these transitions (see, e.g., Figure 4) as well as their overlaps $\rho_o \cdot \rho_t = \rho_{overlap}$ can be plotted in real space to gain more insight. For t = 0 in Figure 3 (upper panel), we see that for the first peak, only the orbitals o = 0 contribute. Thus, transitions at the phenyl substituents for $\rho_{o=0} \cdot \rho_{t=0} = \rho_{o=0,t=0}$ dominate the first peak of the SHG spectrum. Considering the high relative intensity for the first peak, we expect $\rho_{o=0,t=0}$ to be larger than, for example, overlaps $\rho_{o=0,t=2}$, or $\rho_{o=2,t=0}$ correlating with the second peak. This is clearly visible in Figure 5.

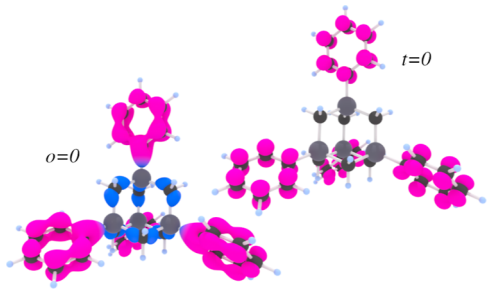

Figure 4. Sum of the squared wave functions ρ calculated for the $[(SiPh)_4(CH_2)_6]$ cluster for o = 0 (lhs) and t = 0 (rhs). ρ is colored from blue to pink as a function of the distance from the core center. H atoms are colored in light blue, the C atoms are black, and the Si atoms are gray.

In Figure 5, overlaps are plotted for the Si-modified structure. A proportionally high volume or magnitude of $\rho_{overlap}$ is interpreted as an indicator for a favorable $o \rightarrow t$ transition if it correlates with a peak in the SHG spectrum. The structural components where $\rho_{overlap}$ is localized most strongly contribute to the SHG spectrum.

It should be noted that a relatively wide orbital group is considered for o = 0, which will increase the probability for an overlap in the charge densities. In Figure 4, the charge density ρ is plotted for o, t = 0. Charge densities are colored by the distance

https://doi.org/10.1021/acsomega.4c08541
ACS Omega 2024, 9, 49816−49824

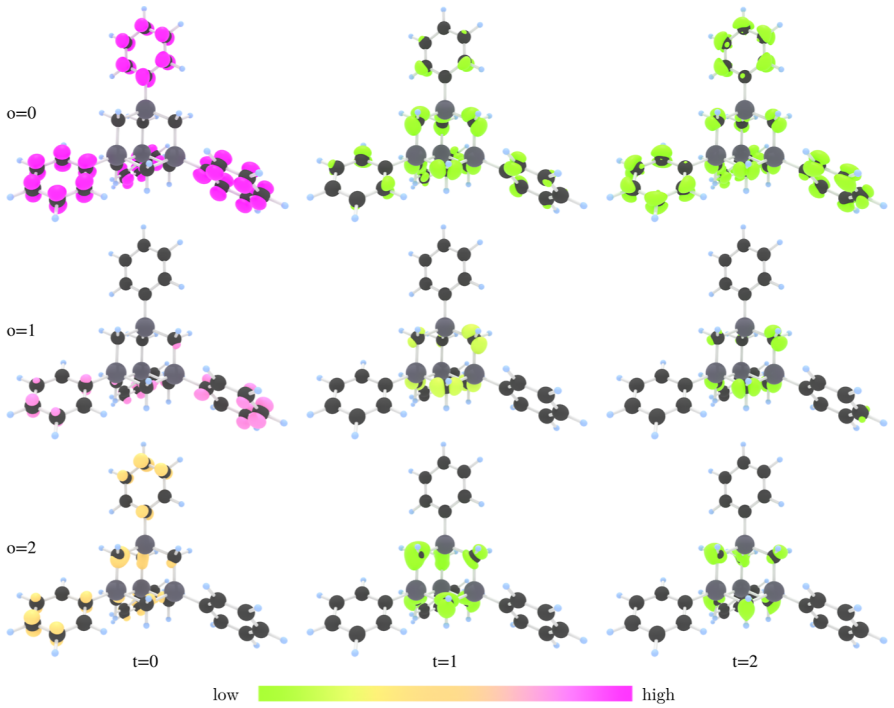

Figure 5. Overlap $\rho_{overlap}$ of *origin* (o) and *target* (t) orbitals, calculated for the $[(SiPh)_4(CH_2)_6]$ cluster, color-coded with respect to the overlap magnitude and normalized by the number of orbitals in the respective orbital groups. C atoms are black and H atoms light blue.

from the middle of the structure. The color is a gradient from blue (core) to pink (substituent). The isosurface shown is dynamically chosen to provide a clear representation of the investigated structures. The values are not normalized for the number of individual orbitals within an orbital group. Thus, the figure is intended to qualitatively show the spatial distribution of origin and target groups and not to yield quantitative and comparable information about their spatial extent.

As shown in Figure 4, not all orbitals in the origin group are located at a substituent; however, the overlap of origin and target atoms are strongly localized at the substituent (see Figure 5), as the target groups are strongly localized at the phenyl rings.

We remark that for the sake of clarity, we do not employ the same isosurface for all the transitions, which would result in a very large volume, e.g., for $o = 0$, $t = 0$, and a vanishing overlap volume, e.g., for $o = 2$, $t = 2$. Instead, we arbitrarily chose an isosurface value so that the overlap region is well visible and color code the isosurface to represent its magnitude. The figure clearly shows that the electronic transitions associated with the peaks of the SHG spectra are localized at the phenyl substituents. This suggests that the optical nonlinearities have their origin in the substituents.

$[(GePh)_4(CH_2)_6]$. The $[(GePh)_4(CH_2)_6]$ cluster features an SHG spectrum very similar to the Si-modified tetraphenyl-adamantane structure, as seen in Figure 2. The Si−C and Ge−C bond lengths are very close, the cluster core volumina are comparable, and an overall similar behavior is expected. The analysis of the electronic states and of the electronic transitions confirms this impression. The electronic structure and the SHG spectrum of the Ge-modified structure are shown in Figure 6, which strongly resemble the previously discussed data calculated for the Si-modified structure. The only appreciable difference is that the topmost three occupied electronic states which were grouped into the group $o = 0$ for the $[(SiPh)_4(CH_2)_6]$ cluster are separated by slightly larger energies and therefore considered distinct origin groups $o = 0$, 1, and 2.

The charge densities of the orbital groups $o = 0$, 1, and 2 are plotted in Figure 7. The color coding and isosurface choice are equivalent to Figure 4.

The sum of all three charge densities shares the characteristics of the charge density for $o = 0$ of Figure 4. A slightly higher localization at the substituents can be observed, which we attribute to the slightly larger Ge−C bond length.

As a consequence, the groups $o = 0$, 1, and 2 together play a role that is comparable to the group $o = 0$ of the $[(SiPh)_4(CH_2)_6]$ structure, as shown in Figure 6, which represents the correlation between electronic energy levels, SHG spectrum, and convolution $o * t$.

The similarity of the $[(SiPh)_4(CH_2)_6]$ and $[(GePh)_4(CH_2)_6]$ clusters is confirmed by the analysis of the orbital overlap associated with the electronic transitions from the origin of the target states. They are displayed in Figure 8.

As in the case of the Si-substituted molecule, the only target group involving transitions associated with the first SHG peak is $t = 0$. Indeed, in Figure 9, where we show the target orbitals $t = 0$ and 1, a clear substituent localization for $t = 0$ can be seen. For $t = 1$, the orbitals are mostly core localized and have a minor overlap with the origin orbitals. They can therefore yield only a minor or no contribution to the SHG signal.

The substituent localized parts of the charge density for $t = 1$ are clearly oriented toward the core. This core-sided localization can be seen in the overlaps for $t = 1$ in Figure 8.

As expected from the evaluation of Figure 6, where it can be seen that the convolutions of the origin states with the target groups $t = 1$ and even more $t = 2$ do not coincide with a peak of the SHG, Figure 8 shows that correspondingly the overlaps for transitions to $t = 1$ and $t = 2$ are of very low magnitude and can only yield a minor contribution to the SHG signal. Altogether, we conclude that $[(SiPh)_4(CH_2)_6]$ and $[(GePh)_4(CH_2)_6]$ have

https://doi.org/10.1021/acsomega.4c08541
ACS Omega 2024, 9, 49816−49824

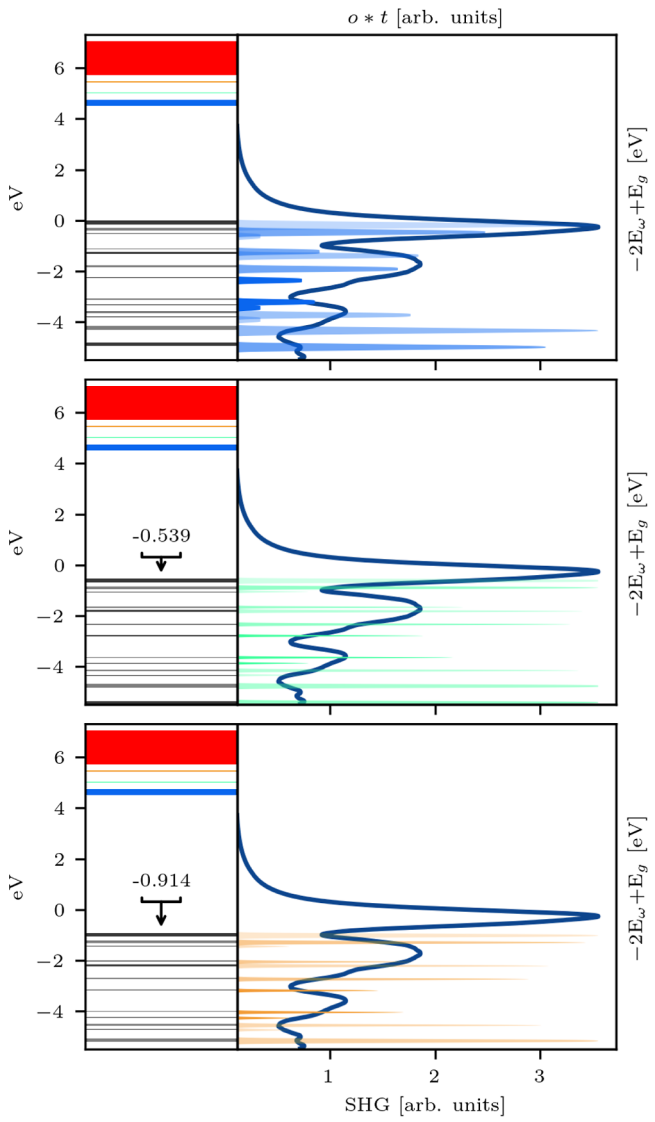

Figure 6. Orbital group energy values of $[(GePh)_4(CH_2)_6]$ with corresponding scaled and shifted SHG response. The energy values of the origin orbital groups are shifted for a direct transition to the respective target orbital groups 0, 1, and 2.

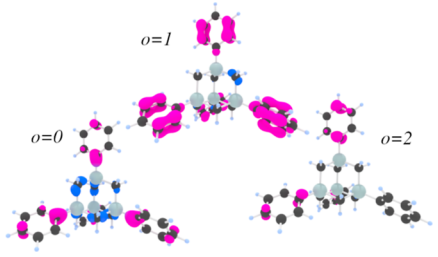

Figure 7. Squared wave functions ρ calculated for the $[(GePh)_4(CH_2)_6]$ cluster for the origin states o = 0, 1, and 2. The coloring of ρ is from blue to pink as a function of the distance from the center of the core. C atoms are black, H atoms light blue, and Ge atoms light gray.

a very similar nonlinear optical response, and its correlation to the electronic and structural properties is practically equivalent in both clusters.

$[(SnPh)_4(CH_2)_6]$. Prior investigations[15,18] have revealed that the tetraphenyl tetrel molecules (and thus such the structures $[SiPh_4]$, $[GePh_4]$, and $[SnPh_4]$ related to the clusters modeled in this work) are rather similar with respect to many properties. Thus, the difference in the SHG response of $[(SnPh)_4(CH_2)_6]$ compared to that of the Si- or Ge-modified structures evokes interest and deserves some attention. A question which we also would like to address is whether the second peak in the SHG spectrum can be interpreted as a signature arising from different electronic transitions compared to the Si- or Ge-modified structures or if it should rather be interpreted as a smearing of the first signature to higher energies due to the spread of the involved electronic states.

Figure 10 shows the correlation between electronic structure, convolution of origin and target states, and SHG spectrum of the $[(SnPh)_4(CH_2)_6]$ cluster. The figure allows us to identify the origin states o = 0, 1, 2, and 3 as possible contributors to the first main SHG peak. As for the target orbital groups, t = 0, 1 needs to be investigated.

To investigate the second peak, we increase the considered energy interval and additionally investigate t = 2 and o = 4 and 5. The presented results for the electronic properties thus take into account o = 0, 1, 2, 3, 4, and 5 and t = 0, 1, and 2. As a comprehensive overlap matrix such as in Figures 5 and 8 is not necessary, we present only selected overlaps with relevant contribution.

Figure 11 shows the localization of the relevant target orbitals t = 0, 1, and 2. For all three orbitals, we see a substituent localization. For t = 0, this is clearly dominant, and no localization is distinguishable, which could be attributed to the core. For t = 1, the majority of the distribution is localized at or toward the core; however, a significant localization at substituents is still present. For t = 2, substituent and core localization are comparable with somewhat higher substituent localization.

For the first major peak in the SHG spectrum, only the transitions into the t = 0 and t = 1 target groups fall within the relevant energy window. Due to the relatively lower contribution for t = 1 to an overlap as suggested by Figure 11, we identify the electronic transitions to t = 0 as the major contributor to the main SHG peak. Independent from the actual origin state (o = 0, 1, 2, and 3), the overlap with the target state t = 0 is localized at the phenyl substituents. In Figure 12, we present the overlaps $\rho_{o=0,t=0}$, $\rho_{o=2,t=0}$, and $\rho_{o=4,t=0}$. The colors represent again the isosurface value. All transitions are characterized by an overlap in the substituent structures. The overlap of highest magnitude among the transitions related to the first SHG peak is calculated for transitions from the orbital group o = 2. These are interestingly exactly the transitions, with an energy corresponding to the maximum of the first SHG peak. The overlap $\rho_{o=0,t=0}$ corresponding to the transition from o = 0 to t = 0 has a lower magnitude and is responsible for the left shoulder of the first major peak. This analysis illustrates well how a quite simple model provides a clear correlation between electronic transitions and SHG spectra, including a qualitative extension of the SHG intensity.

For the second peak, when investigating the transition into t = 0, we identify o = 4 as the major contributor, which also fits well to the convolution o * t shown in Figure 10. Further possible transitions to t = 1 or t = 2 fall in the relevant energy range. The involved origin groups are o = 1, 2, and 3 for transitions to t = 1 and o = 0 and 1 for transitions to t = 2. Using the same scale as that in Figure 12, we report the corresponding overlaps in Figure 13. Only the transition o = 0, t = 2 corresponds to a nonvanishing magnitude, which is, however, lower than those calculated for

https://doi.org/10.1021/acsomega.4c08541
ACS Omega 2024, 9, 49816−49824

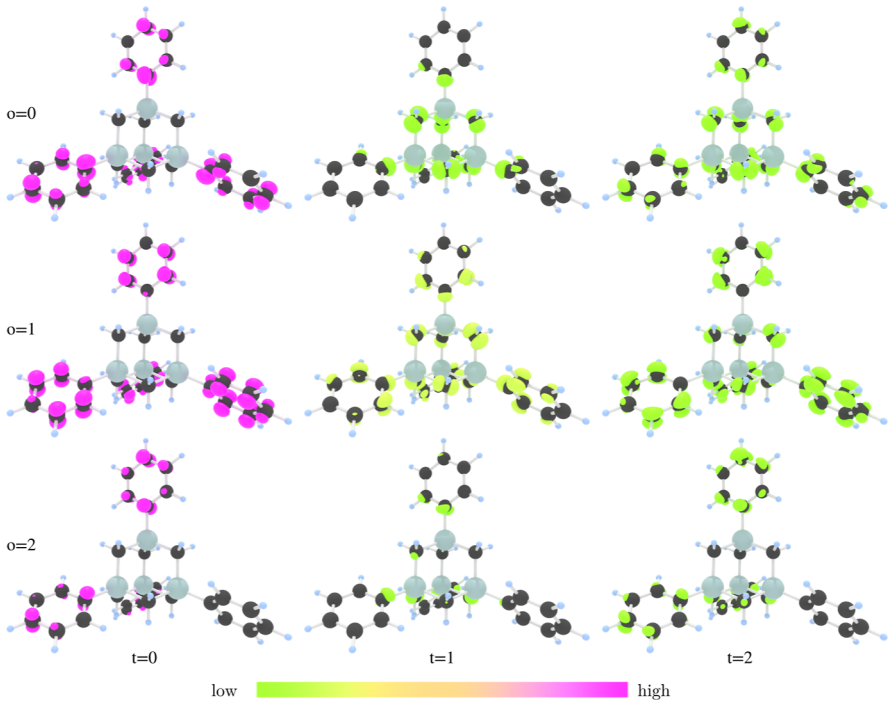

Figure 8. Overlap $\rho_{overlap}$ of *origin* (o) and *target* (t) orbitals, calculated for the $[(GePh)_4(CH_2)_6]$ cluster, color-coded with respect to the overlap magnitude and normalized by the number of orbitals in the respective orbital groups. C atoms are black, H atoms light blue, and Ge light gray.

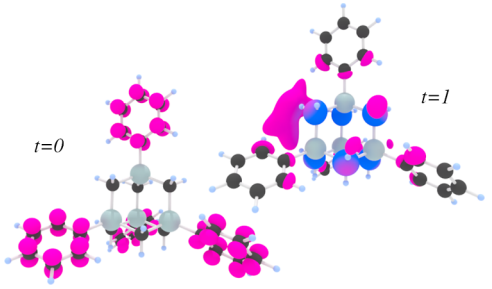

Figure 9. Squared wave functions ρ calculated for the $[(GePh)_4(CH_2)_6]$ cluster for the target states $t = 0$ and 1. Color code of isosurfaces and atoms as in Figure 7.

other electronic transitions (e.g., $o = 4$, $t = 0$ or those associated with the first SHG peak). Due to the substituent localization, we assume that these transitions contribute to the second peak as well; however, the limited overlap results in a lower SHG intensity with respect to the first peak. An overview of the transitions contributing to the different SHG peaks can be found in Figure 14.

The first SHG peak is thus higher in its maximum than the second SHG signature, as more transitions with a large overlap contribute to it. We remark that transitions such as $o = 2$, $t = 0$ which have an energy corresponding to the first SHG peak in the Si-substituted and in the Ge-substituted cluster have energies associated with the second SHG peak in the Sn-substituted cluster. Thus, the spectral weight redistribution that lowers the first SHG peak and enhances the intensity of the second in the Sn-substituted molecule can be viewed as a consequence of electronic energy levels drifting apart. In turn, it explains the apparent deviation of the Sn-substituted cluster from the chemical trend that attributes higher SHG intensity to the cluster substituted with tetrels of higher atomic number.

CONCLUSIONS

The nonlinear optical response of tetraphenyl clusters with the general formula $[(RPh)_4(CH_2)_6]$ and R = C, Si, Ge, and Sn has been calculated from first principles. All clusters feature SHG spectra characterized by corresponding optical signatures, although they might differ to some extent in position and intensity. The spectra are dominated by a main peak at energies corresponding to half of the HOMO−LUMO gap. The SHG intensity related to this peak grows with the atomic number of the considered tetrel. The analysis of the electronic transitions associated with the main SHG peak reveals that the involved orbitals are localized at the substituents. Thus, the origin of the optical nonlinearities in the technologically relevant energy interval from 0 to 3 eV is spatially located at the phenyl rings. On the one hand, this explains why many clusters with tetraphenyl substituents show similar spectra.[1] On the other hand, this confirms the assumption that the presence of delocalized π-orbitals at the substituents is a prerequisite for the high nonlinear optical activity of molecular clusters.[3] The tetrel substitution does not distort the cluster core or lower its symmetry. Thus, the enhanced nonlinear optical activity of clusters with heavier tetrels cannot be explained by softening of the selection rules for the electronic transitions. It is instead attributed to an increased electron density at the substituents, which favors the overlap between occupied and empty orbitals and, thus, the transition between them. A partial substitution of the carbon core atoms by heavier tetrels might well deform the cluster core and thus affect the optical response. This possibility will be the subject of future investigations and is outside the scope of the present investigation, though. Similarly, different substituents (e.g., styrene, methyl, naphtyl, *trans*-stilbene, etc.) with more electron donor or electron-withdrawing character are also expected to heavily impact the SHG response of the clusters.[32] Concerning potential applications, Si-, Ge-, and Sn-substituted adamantane clusters provide highly enhanced SHG intensity and are more

https://doi.org/10.1021/acsomega.4c08541
ACS Omega 2024, 9, 49816−49824

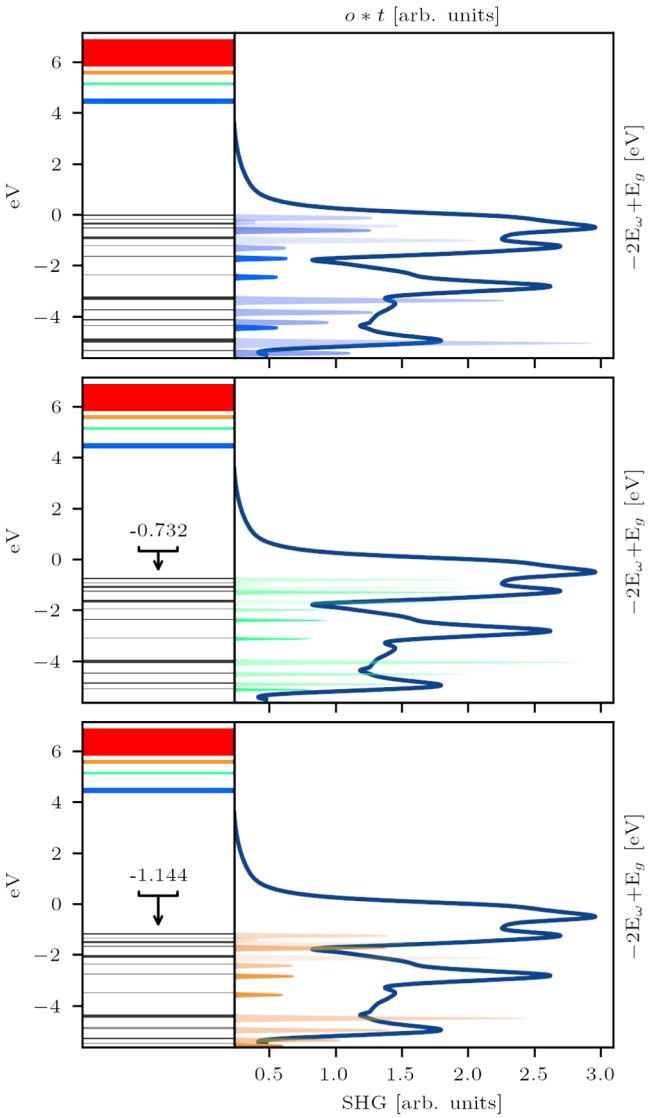

Figure 10. Orbital group energy values of $[(SnPh)_4(CH_2)_6]$ with corresponding scaled and shifted SHG response. The energy values of the origin (occupied) orbital groups are shifted for a direct transition to the respective target (unoccupied) orbital groups 0, 1, 2, and 3.

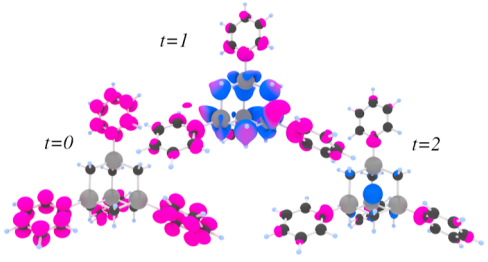

Figure 11. Squared wave functions ρ of the target states $t = 0$, 1, and 2 of the $[(SiPh)_4(CH_2)_6]$ cluster. The color coding of ρ is from blue to pink as a function of the distance from the core center. C atoms are black, H light blue, and Sn gray.

efficient frequency doublers with respect to the prototypical organic $[(CPh)_4(CH_2)_6]$. Sn-substituted materials, in particular, extend the range of efficient SHG generation to almost 3 eV and are thus suitable for devices working with higher frequencies. The present investigation represents a further step toward the understanding of the nonlinear optical response of the materials class with the more general formula $[(RT)_4E_6]$, with R = organic group; T = C, Si, Ge, and Sn; and E = O, S, Se, Te, NH, CH_2, and ON*, and provides a theoretical foundation for the design of materials with tailored nonlinear optical properties.

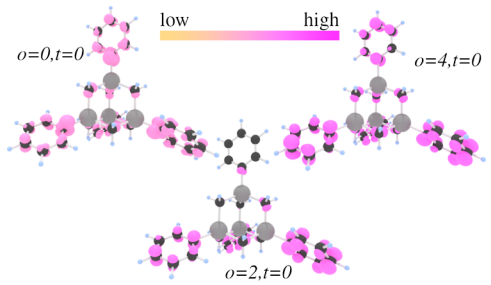

Figure 12. Overlaps of the electronic states $o = 0$, 2, and 4 with $t = 0$ for the $[(SnPh)_4(CH_2)_6]$ cluster. Carbon atoms are black, hydrogen light blue, and Sn gray.

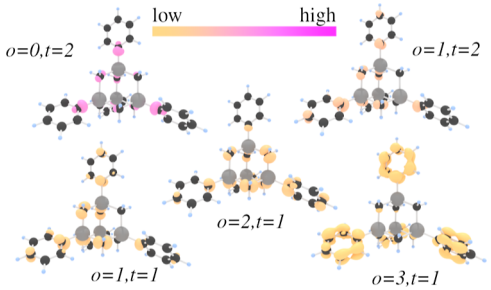

Figure 13. Selected overlaps between origin and target orbitals of the $[(SnPh)_4(CH_2)_6]$ cluster. Color coding as in Figure 12.

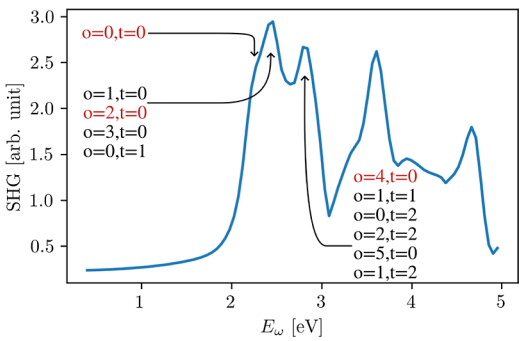

Figure 14. Calculated SHG spectrum of the $[(SnPh)_4(CH_2)_6]$ cluster. Electronic transitions contributing to the low-energy signatures are indicated. The transitions characterized by the largest overlap between origin and target states are marked in red.

■ ASSOCIATED CONTENT

Supporting Information

The Supporting Information is available free of charge at https://pubs.acs.org/doi/10.1021/acsomega.4c08541.

Atom coordinates, procedure to choose main computational parameters for nonlinear optical calculations, further numerical parameters, and description of coloring of the orbital (overlaps) (PDF)

https://doi.org/10.1021/acsomega.4c08541
ACS Omega 2024, 9, 49816−49824

AUTHOR INFORMATION

Corresponding Authors

Ferdinand Ziese − *Institut für Theoretische Physik and Center for Materials Research (LaMa), Justus-Liebig-Universität Gießen, 35392 Gießen, Germany;* orcid.org/0009-0003-6855-9708; Email: ferdinand.ziese@physik.uni-giessen.de

Simone Sanna − *Institut für Theoretische Physik and Center for Materials Research (LaMa), Justus-Liebig-Universität Gießen, 35392 Gießen, Germany;* orcid.org/0000-0003-4416-0252; Email: simone.sanna@theo.physik.uni-giessen.de

Complete contact information is available at: https://pubs.acs.org/10.1021/acsomega.4c08541

Notes

The authors declare no competing financial interest.

ACKNOWLEDGMENTS

This work is supported by the German Research Foundation (DFG) through the research group FOR2824 (Grant No. 398143140, project SA1948/2-2). Calculations for this research were conducted on the Lichtenberg high-performance computer of the TU Darmstadt and at the Höchstleistungrechenzentrum Stuttgart (HLRS). The authors furthermore acknowledge the computational resources provided by the HPC Core Facility and the HRZ of the Justus-Liebig-Universität Gießen.

ADDITIONAL NOTES

[1](This can differ from the displayed lines where we force this delta to be at least $\min(\Delta E)_{\text{vis}} = 0.01$ eV.) We also force a $\min(\Delta E)_{*} = 0.01$ eV, which is used to calculate a convolution (of step functions with the width ΔE) between the origin orbital groups o (being the occupied orbitals) and a specific target orbital group t (being the unoccupied orbitals).
[2]This is skewed for $\min(\Delta E)_{*} = 0.01$ eV.

REFERENCES

(1) Rinn, N.; Rojas-León, I.; Peerless, B.; Gowrisankar, S.; Ziese, F.; Rosemann, N. W.; Pilgrim, W.-C.; Sanna, S.; Schreiner, P. R.; Dehnen, S. Adamantane-type clusters: compounds with a ubiquitous architecture but a wide variety of compositions and unexpected materials properties. *Chem. Sci.* **2024**, *15*, 9438−9509.

(2) Rosemann, N. W.; Eußner, J. P.; Beyer, A.; Koch, S. W.; Volz, K.; Dehnen, S.; Chatterjee, S. A highly efficient directional molecular white-light emitter driven by a continuous-wave laser diode. *Science* **2016**, *352*, 1301−1304.

(3) Dehnen, S.; Schreiner, P. R.; Chatterjee, S.; Volz, K.; Rosemann, N. W.; Pilgrim, W.-C.; Mollenhauer, D.; Sanna, S. Amorphous Molecular Materials for Directed Supercontinuum Generation. *ChemPhotoChem* **2021**, *5*, 1033−1041.

(4) Li, D.; Hu, W.; Wang, J.; Zhang, Q.; Cao, X.-M.; Ma, X.; Tian, H. White-light emission from a single organic compound with unique self-folded conformation and multistimuli responsiveness. *Chem. Sci.* **2018**, *9*, 5709−5715.

(5) Rosemann, N. W.; Eußner, J. P.; Dornsiepen, E.; Chatterjee, S.; Dehnen, S. Organotetrel Chalcogenide Clusters: Between Strong Second-Harmonic and White-Light Continuum Generation. *J. Am. Chem. Soc.* **2016**, *138*, 16224−16227.

(6) Wu, J.; Zheng, G.; Liu, X.; Qiu, J. Near-infrared laser driven white light continuum generation: materials, photophysical behaviours and applications. *Chem. Soc. Rev.* **2020**, *49*, 3461−3483.

(7) Schütt, F.; Zapf, M.; Signetti, S.; Strobel, J.; Krüger, H.; Röder, R.; Carstensen, J.; Wolff, N.; Marx, J.; Carey, T.; et al. Conversionless efficient and broadband laser light diffusers for high brightness illumination applications. *Nat. Commun.* **2020**, *11*, 1437.

(8) Stellhorn, J. R.; Hayakawa, S.; Klee, B. D.; Paulus, B.; Link Vasco, J.; Rinn, N.; Rojas León, I.; Hosier, C. A.; Dehnen, S.; Pilgrim, W.-C. Local Cluster Distortions in Amorphous Organotin Sulfide Compounds and Their Influence on the Nonlinear Optical Properties. *Adv. Opt. Mater.* **2023**, *11*, 2201932.

(9) Peters, B.; Lichtenberger, N.; Dornsiepen, E.; Dehnen, S. Current advances in tin cluster chemistry. *Chem. Sci.* **2020**, *11*, 16−26.

(10) Cole, J. M. Organic materials for second-harmonic generation: advances in relating structure to function. *Philos. Trans. R. Soc., A* **2003**, *361*, 2751−2770.

(11) Dornsiepen, E.; Dobener, F.; Mengel, N.; Lenchuk, O.; Dues, C.; Sanna, S.; Mollenhauer, D.; Chatterjee, S.; Dehnen, S. White-Light Generation Upon In-Situ Amorphization of Single Crystals of $[(Me_3P)_3AuSn(PhSn)_3S_6]$ and $[(Et_3P)_3AgSn(PhSn)_3S_6]$. *Adv. Opt. Mater.* **2019**, *7*, 1801793.

(12) Müller, M. J.; Ziese, F.; Belz, J.; Hüppe, F.; Gowrisankar, S.; Bernhardt, B.; Schwan, S.; Mollenhauer, D.; Schreiner, P. R.; Volz, K.; Sanna, S.; Chatterjee, S. Octave-spanning emission across the visible spectrum from single crystalline 1,3,5,7-tetrakis-(p-methoxyphenyl)-adamantane. *Opt. Mater. Express* **2022**, *12*, 3517−3529.

(13) Belz, J.; Haust, J.; Müller, M. J.; Eberheim, K.; Schwan, S.; Gowrisankar, S.; Hüppe, F.; Beyer, A.; Schreiner, P. R.; Mollenhauer, D.; Sanna, S.; Chatterjee, S.; Volz, K. Adamantanes as White-Light Emitters: Controlling the Arrangement and Functionality by External Coulomb Forces. *J. Phys. Chem. C* **2022**, *126*, 9843−9854.

(14) Schwan, S.; Achazi, A. J.; Ziese, F.; Schreiner, P. R.; Volz, K.; Dehnen, S.; Sanna, S.; Mollenhauer, D. Insights into molecular cluster materials with adamantane-like core structures by considering dimer interactions. *J. Comput. Chem.* **2023**, *44*, 843−856.

(15) Eberheim, K.; Dues, C.; Attaccalite, C.; Müller, M. J.; Schwan, S.; Mollenhauer, D.; Chatterjee, S.; Sanna, S. Tetraphenyl Tetrel Molecules and Molecular Crystals: From Structural Properties to Nonlinear Optics. *J. Phys. Chem. C* **2022**, *126*, 3713−3726.

(16) Rojas-León, I.; Christmann, J.; Schwan, S.; Ziese, F.; Sanna, S.; Mollenhauer, D.; Rosemann, N. W.; Dehnen, S. Cluster-Glass for Low-Cost White-Light Emission. *Adv. Mater.* **2022**, *34*, 2203351.

(17) Hanau, K.; Schwan, S.; Schäfer, M. R.; Müller, M. J.; Dues, C.; Rinn, N.; Sanna, S.; Chatterjee, S.; Mollenhauer, D.; Dehnen, S. Towards Understanding the Reactivity and Optical Properties of Organosilicon Sulfide Clusters. *Angew. Chem., Int. Ed.* **2021**, *60*, 1176−1186.

(18) Ziese, F.; Wang, J.; Rojas León, I.; Dehnen, S.; Sanna, S. Origin of the non-linear optical response in organotetrel molecules, (hetero)-adamantane-type clusters with organic substituents, and related species. *J. Phys. Chem. C* **2024**, *128*, 8360−8372.

(19) Silva, P. S. P.; El Ouazzani, H.; Pranaitis, M.; Silva, M. R.; Arranja, C.; Sobral, A.; Sahraoui, B.; Paixão, J. A. Experimental and theoretical studies of the second- and third-order NLO properties of a semi-organic compound: 6-Aminoquinolinium iodide monohydrate. *Chem. Phys.* **2014**, *428*, 67−74.

(20) Spiridon, M. C.; Iliopoulos, K.; Jerca, F. A.; Jerca, V. V.; Vuluga, D. M.; Vasilescu, D. S.; Gindre, D.; Sahraoui, B. Novel pendant azobenzene/polymer systems for second harmonic generation and optical data storage. *Dyes Pigm.* **2015**, *114*, 24−32.

(21) Sahraoui, B.; Czaplicki, R.; Klöpperpieper, A.; Andrushchak, A. S.; Kityk, A. V. Ferroelectric $AgNa(NO_2)_2$ crystals as novel highly efficient nonlinear optical material: Phase matched second harmonic generation driven by a spontaneous and electric field induced polarizations. *J. Appl. Phys.* **2010**, *107*, 113526.

(22) Sangalli, D.; Ferretti, A.; Miranda, H.; Attaccalite, C.; Marri, I.; Cannuccia, E.; et al. Many-body perturbation theory calculations using the yambo code. *J. Phys.: Condens. Matter* **2019**, *31*, 325902.

(23) Attaccalite, C.; Grüning, M. Nonlinear optics from an ab initio approach by means of the dynamical Berry phase: Application to second- and third-harmonic generation in semiconductors. *Phys. Rev. B* **2013**, *88*, 235113.

(24) Giannozzi, P.; Andreussi, O.; Brumme, T.; Nardelli, M. B.; Calandra, M.; Car, R.; et al. Advanced capabilities for materials

https://doi.org/10.1021/acsomega.4c08541
ACS Omega 2024, 9, 49816−49824

modelling with QUANTUM ESPRESSO. *J. Phys.: Condens. Matter* **2017**, *29*, 465901.
(25) Giannozzi, P.; Baroni, S.; Bonini, N.; Calandra, M.; Car, R.; Cavazzoni, C.; et al. QUANTUM ESPRESSO: a modular and open-source software project for quantum simulations of materials. *J. Phys.: Condens. Matter* **2009**, *21* (19), 395502.
(26) Hamann, D. R. Optimized norm-conserving Vanderbilt pseudopotentials. *Phys. Rev. B* **2013**, *88*, 085117.
(27) Schlipf, M.; Gygi, F. Optimization algorithm for the generation of ONCV pseudopotentials. *Comput. Phys. Commun.* **2015**, *196*, 36−44.
(28) Perdew, J. P.; Burke, K.; Ernzerhof, M. Generalized Gradient Approximation Made Simple. *Phys. Rev. Lett.* **1996**, *77*, 3865−3868.
(29) Grimme, S.; Antony, J.; Ehrlich, S.; Krieg, H. A consistent and accurate ab initio parametrization of density functional dispersion correction (DFT-D) for the 94 elements H-Pu. *J. Chem. Phys.* **2010**, *132*, 154104.
(30) Grimme, S.; Ehrlich, S.; Goerigk, L. Effect of the damping function in dispersion corrected density functional theory. *J. Comput. Chem.* **2011**, *32*, 1456−1465.
(31) Wang, J.; Rojas-León, I.; Rinn, N.; Guggolz, L.; Ziese, F.; Sanna, S.; Rosemann, N. W.; Dehnen, S. Strain-Induced Structural Rearrangement Towards a White-Light-Emitting Adamantane-Type Cluster Dimer. *Angew. Chem., Int. Ed.* **2024**, No. e202411752.
(32) Kulyk, B.; Guichaoua, D.; Ayadi, A.; El-Ghayoury, A.; Sahraoui, B. Functionalized azo-based iminopyridine rhenium complexes for nonlinear optical performance. *Dyes Pigm.* **2017**, *145*, 256−262.

https://doi.org/10.1021/acsomega.4c08541
ACS Omega 2024, 9, 49816−49824